



Deformation experiments using synchrotron X-rays: in situ stress and strain measurements at high pressure and temperature

Jiuhua Chen*, Li Li¹, Donald Weidner², Michael Vaughan³

*Department of Geosciences, Mineral Physics Institute, State University of New York at Stony Brook,
Stony Brook, NY 11794-2100, USA*

Received 31 January 2003; received in revised form 2 August 2003; accepted 21 September 2003

Abstract

An experimental technique for in situ stress and strain measurements at high pressure and temperature using synchrotron X-rays has been developed at the X17B beamline of the National Synchrotron Light Source. The strain is measured by correlating sample-length marks in recorded X-ray radiographs. The stress is measured by simultaneously collecting energy-dispersive X-ray diffraction patterns of the sample in two perpendicular diffraction planes. Differential stress in the sample is derived from the different lattice strains along the different orientations relative to principal stress direction. Example measurements are conducted to study rheological properties of fayalite. Accuracy of the measurement is about 10–100 MPa for stress and about 10^{-4} for strain.

© 2004 Elsevier B.V. All rights reserved.

Keywords: Deformation; High pressure; X-ray diffraction; X-ray imaging; Fayalite; Rheology

1. Introduction

Rheological properties of minerals are very important parameters for understanding Earth's dynamic phenomena such as mantle convection and deep focus earthquakes. As mechanisms of deformation in minerals change with pressure and temperature, rheology studies at mantle conditions are essential to understand the mineral's behavior in the Earth's interior. However, technical difficulties up to now

have prevented us from conducting conventional stress–strain rate deformation experiments at pressures above ~ 3 GPa (Tingle et al., 1993). Recent developments with a multi anvil press have made significant progress in carrying out deformation experiments at higher pressures (Durham and Rubie, 1998; Yamazaki et al., 1996; Bussod et al., 1993; Liebermann et al., 1992; Green et al., 1990). Karato and Rubie (Karato and Rubie, 1997) designed a cell assembly with a thin sample sandwiched between two pistons at 45° angle to their long axis for deformation studies up to 15 GPa. Weidner et al., (Weidner, 1998; Weidner et al., 1998) developed an analytical method to measure the microscopic stress in powder sample by deconvoluting X-ray diffraction peak broadening at the pressure of 20 GPa. However, none of these experimental systems is a direct extension of the traditional macroscopic strain and stress measurement.

* Corresponding author. Tel.: +1-631-632-8058;
fax: +1-631-632-8140.

E-mail addresses: jiuhua.chen@sunysb.edu (J. Chen),
lilli@ic.sunysb.edu (L. Li), donald.weidner@sunysb.edu
(D. Weidner), michael.vaughan@sunysb.edu (M. Vaughan).

¹ Tel.: +1-631-632-8220; fax: +1-631-632-8140.

² Tel.: +1-631-632-8211; fax: +1-631-632-8140.

³ Tel.: +1-631-632-8238; fax: +1-631-632-8140.

Estimation of the stress during deformation at high pressure and temperature (Karato and Rubie, 1997) or assumption of a constant total strain (Weidner, 1998) introduce additional uncertainties for constructing a flow law from their experimental data. On the other hand, measuring sample stress in an opposed anvil apparatus (Drickamer-type and diamond anvil cell) using X-ray diffraction has been reported to investigate strength or stress distribution of samples at high pressures far beyond 20 GPa (Kavner and Duffy, 2001; Mao et al., 1998; Uchida et al., 1997; Funamori et al., 1994). But the very thin sample thickness in this type of apparatus restricts its application in deriving deformation flow laws through strain rate and stress data.

The limitation in maximum pressure of a conventional deformation apparatus is due to the limited strength of the unsupported mobile piston and the difficulty of modeling a supported mobile piston in stress calculation. To challenge this problem, developments have been made to avoid the mobile piston in a high pressure apparatus, e.g. Yamazaki and Karato (Yamazaki and Karato, 2001) modified a Drickamer apparatus to generate large rotational strains at high pressure up to 15 GPa.

We have developed a new technique for performing the conventional deformation experiments using a multi anvil apparatus in conjunction with a synchrotron X-ray source. Sample strain is measured through a direct sample-length imaging system; and stress is derived through multiple X-ray diffraction measurements of the sample along different orientation relative to the principal stress axis. With this technique, sample strain and stress are directly measured independent of the process of strain and stress delivery through the piston. Therefore, the deformation piston can be supported by the surrounding pressure medium so that the pressure can reach far beyond the yield strength of the piston. Since the actual sample length is monitored throughout the experiment, one can easily distinguish the initial deformation during pressurization and the plastic deformation at high pressure and temperature, which has been a critical problem in the recent challenge deformation experiments at high pressures (Durham and Rubie, 1998; Karato and Rubie, 1997; Yamazaki et al., 1996; Bussod et al., 1993; Liebermann et al., 1992; Green et al., 1990). The

experiment described in this paper is carried out using a regular single ram multi-anvil press, therefore the deformation cycles are limited to stress relaxation. Applying this technique to a newly developed Deformation-DIA type press (Wang et al., 2004), one can conduct a typical constant strain rate deformation while accurately monitor the sample stress and strain rate.

2. Lattice strain measured using X-ray diffraction

2.1. The expression

Expressions for lattice strains produced by nonhydrostatic pressure depend on the diffraction geometry in the high pressure experiment (Singh, 1993). For a multi anvil press, the common geometry is illustrated in Fig. 1, in which the incident X-ray beam for diffraction is perpendicular to the principal loading (σ) direction (vertical axis in the laboratory coordinate system). If we let ψ be the angle between this principal loading direction and the diffraction vector (normal to the crystallographic plane (hkl) that diffracts the X-ray), we have $\psi = \theta$ (Bragg angle) for the diffracted X-rays in the vertical diffraction plane and $\psi = \pi/2$ for those in the horizontal diffraction plane. Assuming a cylindrical symmetry of the stress field in a multi anvil cell, i.e. $\sigma_1 = \sigma_2 \neq \sigma_3$, we can describe the stress at the

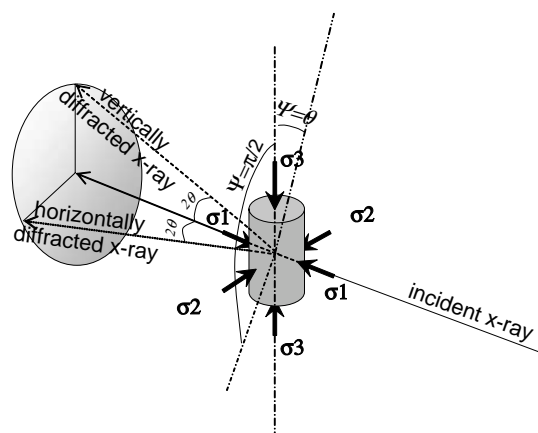


Fig. 1. Common geometry of X-ray diffraction and stress field in a multi anvil high pressure apparatus. θ the Bragg angle of the X-ray diffraction, ψ the angle between diffraction vector and principal stress (σ_3) axis.

center of the sample by

$$\sigma_{ij} = \begin{pmatrix} \sigma_1 & 0 & 0 \\ 0 & \sigma_1 & 0 \\ 0 & 0 & \sigma_3 \end{pmatrix} = \begin{pmatrix} \sigma_p & 0 & 0 \\ 0 & \sigma_p & 0 \\ 0 & 0 & \sigma_p \end{pmatrix} + \begin{pmatrix} -t/3 & 0 & 0 \\ 0 & -t/3 & 0 \\ 0 & 0 & 2t/3 \end{pmatrix} \quad (1)$$

where σ_1 and σ_3 are radial and axial stress components, respectively, σ_p the mean normal stress (hydrostatic pressure), t the differential stress, and

$$\sigma_p = \frac{1}{3}(\sigma_1 + \sigma_2 + \sigma_3) = \frac{1}{3}(2\sigma_1 + \sigma_3) \quad (2)$$

$$t = \sigma_3 - \sigma_1 \quad (3)$$

Under this assumption, the expression for lattice strain $\varepsilon(hkl)$ becomes similar to that of the “perpendicular geometry” (PD-G, or the incident X-ray beam is perpendicular to the load direction) in opposed anvil device (Singh et al., 1998; Singh, 1993), and is given by

$$\varepsilon(hkl) = \varepsilon_p + \frac{1}{3}t(1 - 3\cos^2\psi)\{\alpha[2G_R(hkl)]^{-1} + (1 - \alpha)(2G_V)^{-1}\} \quad (4)$$

where ε_p is strain due to the hydrostatic pressure component in the total stress, $G_R(hkl)$ is the aggregate shear modulus calculated under the Reuss (iso-stress) condition, G_V is the shear modulus under the Voigt (iso-strain) condition, and α is a weight parameter of Reuss and Voigt condition for a real polycrystalline sample. The Reuss aggregate shear modulus is expressed as the following equation (Singh et al., 1998) for a general crystal system (triclinic symmetry: $a \neq b \neq c$, $\alpha \neq \beta \neq \gamma \neq 90^\circ$),

$$\begin{aligned} & [2G_R(hkl)]^{-1} \\ &= \frac{1}{2}[S_{11}(3l_1^4 - l_1^2) + S_{12}(6l_1^2l_2^2 - l_1^2 - l_2^2) \\ &+ S_{13}(6l_1^2l_3^2 - l_1^2 - l_3^2) \\ &+ (S_{14}l_2l_3 + S_{15}l_3l_1 + S_{16}l_1l_2)(6l_1^2 - 1) \\ &+ S_{22}(3l_2^4 - l_2^2) + S_{23}(6l_2^2l_3^2 - l_2^2 - l_3^2) \\ &+ (S_{24}l_2l_3 + S_{25}l_3l_1 + S_{26}l_1l_2)(6l_2^2 - 1) \\ &+ S_{33}(3l_3^4 - l_3^2) + (S_{34}l_2l_3 + S_{35}l_3l_1 + S_{36}l_1l_2) \\ &\times (6l_3^2 - 1) + 3S_{44}l_2^2l_3^2 + 6(S_{45}l_3 + S_{46}l_2)l_1l_2l_3 \\ &+ 3S_{55}l_3^2l_1^2 + 6S_{56}l_1^2l_2l_3 + 3S_{66}l_1^2l_2^2] \end{aligned} \quad (5)$$

where S_{ij} are elastic compliances at the pressure σ_p , $l_1 = (hb - ak \cos \gamma)d(hkl)/ab \sin \gamma$, $l_2 = kd(hkl)/b$ and $l_3 = (Y/Z)d(hkl)$. Y and Z are defined by $Y = abl \sin^2 \gamma + bch(\cos \alpha \cos \gamma - \cos \beta) + ack(\cos \beta \cos \gamma - \cos \alpha)$ and $Z = abc(1 - \cos^2 \alpha - \cos^2 \beta - \cos^2 \gamma + 2 \cos \alpha \cos \beta \cos \gamma)^{1/2} \sin \gamma$.

The Voigt shear modulus is given by

$$G_V = \frac{1}{15}(C_{11} + C_{22} + C_{33} - C_{12} - C_{23} - C_{31} + 3C_{44} + 3C_{55} + 3C_{66}) \quad (6)$$

where C_{ij} are elastic stiffness (Hearmon, 1956).

2.2. Determining ε_p , t and α experimentally

Collecting X-ray diffraction data at different ψ angles is indispensable for determining ε_p , t and α through Eq. (4). If we let ε_H and ε_V represent the strain measured at $\psi = \pi/2$ and $\psi = 0$, Eq. (4) becomes,

$$\varepsilon_H(hkl) = \varepsilon_p + \frac{1}{3}t\{\alpha[2G_R(hkl)]^{-1} + (1 - \alpha)(2G_V)^{-1}\} \quad (7)$$

and

$$\varepsilon_V(hkl) = \varepsilon_p - \frac{2}{3}t\{\alpha[2G_R(hkl)]^{-1} + (1 - \alpha)(2G_V)^{-1}\} \quad (8)$$

Therefore,

$$\varepsilon_p = \frac{1}{3}(2\varepsilon_H + \varepsilon_V) \quad (9)$$

From Eq. (7) and (8), we also obtain

$$\begin{aligned} \Delta\varepsilon(hkl) &\equiv \varepsilon_H(hkl) - \varepsilon_V(hkl) \\ &= t\alpha[2G_R(hkl)]^{-1} + t(1 - \alpha)(2G_V)^{-1} \end{aligned} \quad (10)$$

Plotting the observed $\Delta\varepsilon(hkl)$ for each diffraction peak (hkl) as a function of $[2G_R(hkl)]^{-1}$, we can derive t and α

$$t = a + 2bG_V \quad (11)$$

$$\alpha = \frac{a}{a + 2bG_V} \quad (12)$$

where a and b are the slope and the intercept of $\Delta\varepsilon(hkl)$ axis of the plot, respectively. To obtain the value of t and α through this approach, elastic compliances S_{ij} of the sample at the pressure and temperature are required.

In many cases, however, the pressure and temperature dependences of the elastic compliances are unknown. Singh et al. (Singh et al., 1998) and Uchida et al. (Uchida et al., 1996) discussed the possibilities of estimating t for different crystal structure systems. For an elastically isotropic cubic material, t can be estimated (Singh et al., 1998) by

$$t = 6\langle Q(hkl) \rangle G \quad (13)$$

where $\langle \rangle$ denotes the average value for all lattice reflections, G is the shear modulus at the pressure, and $Q(hkl)$ can be derived by plotting $d(hkl)$ versus $1 - 3 \cos^2 \psi$ according to the following equation (Singh et al., 1998),

$$d_m(hkl) = d_p(hkl)[1 + (1 - 3 \cos^2 \psi)Q(hkl)] \quad (14)$$

In X-ray diffraction experiments, $\varepsilon(hkl)$ is not actually measured at $\psi = 0$. As shown in Fig. 1, energy dispersive diffraction patterns collected in the vertical diffraction has $\psi = \theta$. From Eq. (4), we know $\varepsilon(hkl)$ is linear to $1 - 3 \cos^2 \psi$. Therefore, $\varepsilon_V(hkl)$ can be derived (Funamori et al., 1994) by

$$\varepsilon_V(hkl) = \frac{\varepsilon_{\psi=\theta}(hkl) - \varepsilon_H(hkl)\sin^2\theta}{\cos^2\theta} \quad (15)$$

If the Bragg angle (θ) is small, e.g. $\sim 3.2^\circ$ in our experiments, difference between $\varepsilon_V(hkl)$ and $\varepsilon_{\psi=\theta}(hkl)$ is negligible.

3. The experimental setup

The experimental system is installed at the X17B beamline of the National Synchrotron Light Source (NSLS). Experiments are conducted using high energy white X-rays from the superconductor wiggler of X17. Key elements of the experimental system are sketched in Fig. 2. An upstream aperture sets the size of X-rays coming into the experimental hutch. A set of incident slits defines the size of incident X-rays to the sample. The slits are mounted on a motor driven stage, so that they can be moved in and out of the position to change the incident beam size according to the type of measurements. Typically, the upstream aperture sets a $2 \text{ mm} \times 2 \text{ mm}$ beam size for sample imaging, and the slits further define a $100 \mu\text{m} \times 100 \mu\text{m}$ beam size for X-ray diffraction.

A 6–8 double-stage multi anvil high pressure module (Tcup), which can generate high pressure beyond 20 GPa (Vaughan et al., 1998), is used for the deformation experiment. With 8 WC second-stage cubes ($10 \text{ mm} \times 10 \text{ mm} \times 10 \text{ mm}$), the Tcup module typically leaves only one accessible diffraction-plane which is inclined about 35° from the vertical axis (Fig. 3). To gain the accessibility for diffracted X-rays, we replace 6 of the 8 WC cubes (the top and bottom ones are used for passing the heating current to the cell assembly) with sintered cBN cubes. Because of the low X-ray absorption of boron nitride, diffracted X-rays can be measured in the diffraction plane with any angle to the vertical axis. Fig. 4 shows a radiograph of a sample in the cBN anvils. The maximum intensity reduction

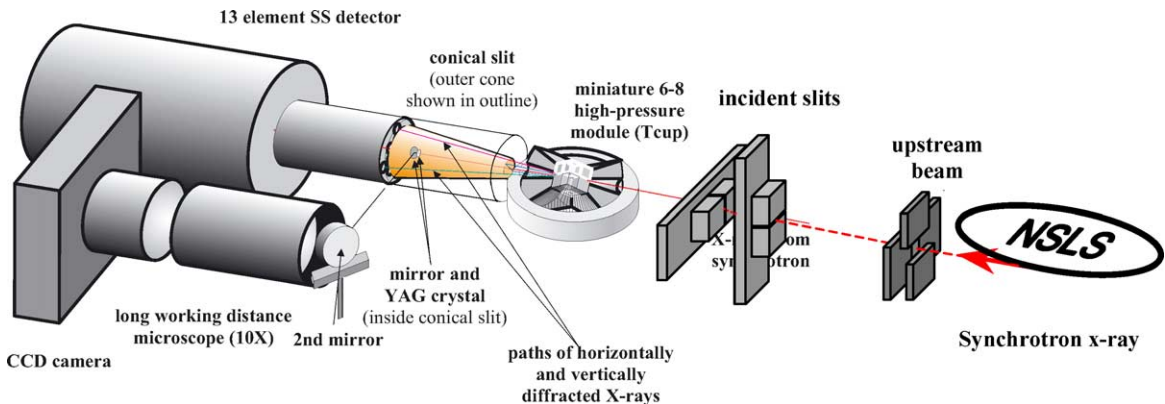


Fig. 2. Layout of the experimental system at X17B of the NSLS for deformation study.

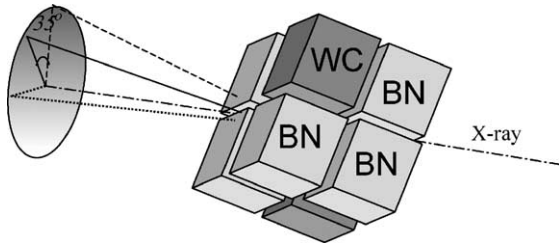


Fig. 3. Diffraction geometry in Tcup module. Solid line indicates the access of diffracted X-rays if all 8 s-stage cubes are made of WC, broken line and dotted line indicate the diffraction in vertical plane and horizontal plane penetrating through BN side cubes.

of the transmitted X-rays by the cBN anvils is about 20%.

A 13-element solid state detector is used to record the energy dispersive X-ray diffraction patterns. The diffracted X-rays are collimated by using a conic slit and detected on four of the 13 detector elements in the vertical and horizontal planes simultaneously (Fig. 5). The conic slit consists of an inner conical block with flat tip and two outer rings. The two rings have different inner diameters and their inner surfaces are tapered to match the conical angle of the inner block. They are attached onto the inner block at about 10 mm apart, as shown in Fig. 5. Spacer shims (typically 50 μm thickness) set a gap between the inner block and outer rings to collimate the diffracted X-rays into the detector. Flux of the diffracted X-rays into the detector is controlled by an aperture placed in between the conic slit and the detector. The aperture consists of two identical four-hole rotational W plates, and the degree of overlapping the holes on the two plates controls the photon flux (see inset of Fig. 5). The mechanical conic

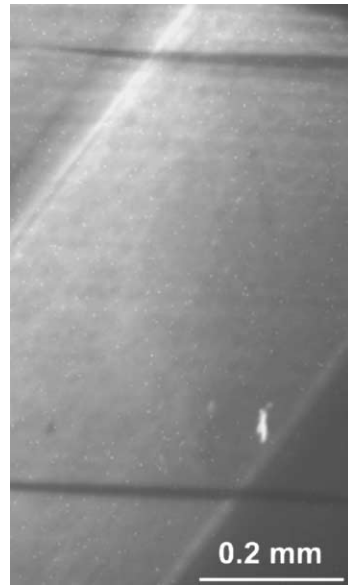


Fig. 4. Radiograph image of fayalite sample and cBN anvils. The bright strip-shape area from top-right to bottom-left indicates the anvil gap. The two horizontal dark lines are the gold foils at each end of the cylindrical sample. Note the dark lines are visible in the anvil areas (grey triangle areas at top-left corner and bottom-right corner).

angle of the inner block is 6.5°, but the actual Bragg angle for each detector depends on the alignment of the slit relative to the incident X-ray. Calibrations of the Bragg angle of each detector are made using X-ray diffraction standard at beginning of the experiment. Fig. 6 shows a typical X-ray diffraction pattern with a data collection time of 95 s.

Both inner conical block and outer rings are made of tungsten-containing brass. The inner conical block

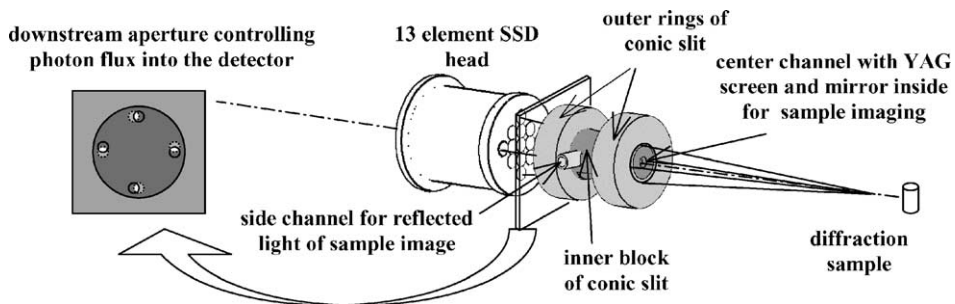


Fig. 5. Conic slit collimating the diffracted X-ray for simultaneous diffraction collection in vertical and horizontal plane with 13-element solid state detector.

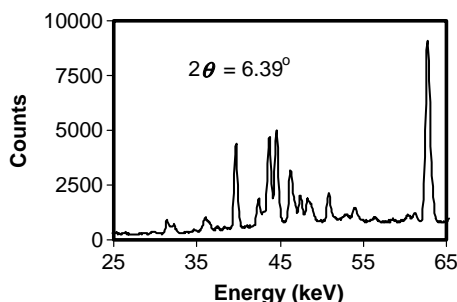


Fig. 6. A typical energy-dispersive X-ray diffraction pattern of fayalite collected at 4.5 GPa and 973 K. The diffracted X-rays transmit through the cBN anvil in the vertical diffraction plane. Data collection time is 95 s.

has two connected holes, one along its axis and one at the side, for accessing of the sample imaging system (see Figs. 2 and 5). A YAG crystal fluorescent screen (6 mm diameter and 100 μm thickness) is mounted in the center hole of the conic slit near the downstream end, perpendicular to the incident X-ray. A mirror is placed at the end of the center hole to reflect visible light from the fluorescent screen to the side channel. Transmitted X-rays through the sample impinge on the fluorescent screen where an image of the sample is generated. Visible light from the sample image are reflected by the mirror in the center hole and the outside mirror, into a CCD camera through a long focusing-distance microscope (Fig. 2). Sample strain is derived from the image of two strain marks (6 μm thick gold foils) placed at both ends of the sample (see Fig. 7 for the cell assembly and Fig. 4 for sample image).

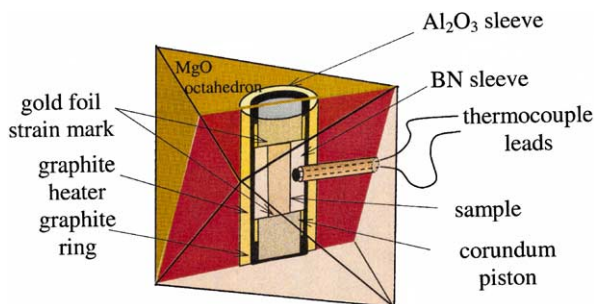


Fig. 7. Cell assembly for high pressure deformation experiments in double-stage Tcup apparatus.

4. The experiment and results

The experimental system has been used to study the deformation of olivine samples. The result on pressure dependence of San Carlos olivine rheology can be found in this volume as a separate report by Li et al. (2004) Here we describe a multiple heating cycle experiment on fayalite, during which the sample transforms from olivine to spinel structure.

Synthetic Fe_2SiO_4 sample is powdered to an average grain size of $\sim 1 \mu\text{m}$, and packed into a cylindrical BN sample chamber of 1 mm diameter and 3 mm length. As shown in Fig. 7, the sample is loaded into an 8 mm edge-length octahedral MgO pressure medium, between two hard corundum pistons. A 6 μm thick gold foil is placed between the sample and the piston at each end as strain mark. Edge-length of the truncation on the second stage anvil is 2 mm.

The sample is first compressed at room temperature and then heated to 973 K to sinter the powder sample. After quenching to room temperature, the sample is further compressed to a higher pressure followed by a second heating. A total of four heating cycles are conducted, each at a higher pressure with respect to previous heating. The sample length is measured directly from the distance between two strain marks at each side of the sample on the X-ray radiograph image of the high pressure cell. The change in sample length during the experiment is shown in Fig. 8. Accuracy of the absolute sample length is influenced by the

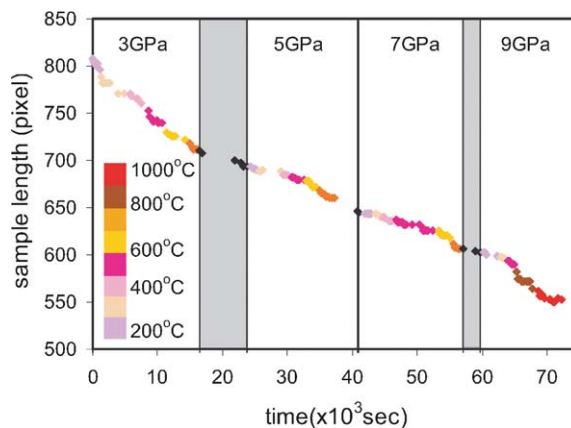


Fig. 8. Change in sample length during the experiment. Pressure and temperature are as indicated. The shaded areas indicate compression periods.

clearness and thickness of the strain mark image (usually in the order of microns). However, a technique of correlating the same strain mark in two consecutive images (Li et al., 2003) increases the accuracy of relative displacement of the strain mark to a fraction of one micron. Therefore, for a sample with about 1 mm length, the strain measurement is accurate to 10^{-4} and strain rate is accurate to 10^{-7} – 10^{-6} depending on the time interval between two measurements. As shown in Fig. 8, each heating cycle generates about 10% total plastic strain.

In calculation the stress of olivine phase, we use the elastic constants of single crystal fayalite and their pressure and temperature dependencies reported by Graham et al. (1988). Single crystal elastic constants and their pressure/temperature dependencies of Fe_2SiO_4 spinel phase are not available. We, therefore, use Eq. (13) to derive the stress in the spinel phase using the shear modulus and its pressure dependence values (87.5 GPa and 0.44) suggested by Hofmeister and Mao (Hofmeister and Mao, 2001). In most cases, diffraction peaks (0 3 1), (2 2 0), (1 3 1), (2 1 1), (0 4 1), (3 1 1), (1 5 1) and (2 2 2) are used in the stress calculation for olivine phase, and diffraction peaks (2 2 0), (3 1 1), (2 2 2), (4 0 0), (3 3 1), (5 1 1) and (4 4 0) are used for spinel phase. Fig. 9 shows the calculated apparent pressures based the diffraction in vertical plane ($\psi = 3.2^\circ$) and in horizontal plane ($\psi = 90^\circ$), the derived effective hydrostatic pressure and the differential stress during the first annealing process.

Because of the hard pistons in the high pressure cell, the apparent pressure along the piston axis increases dramatically whereas that along the direction perpendicular to this axis barely increases during the initial compression. This indicates that huge differential stress builds up in the sample. Clearly, none of these apparent pressures represent the true pressure in the sample. The effective hydrostatic pressure lies between the two apparent pressures. Upon heating, the apparent pressure along the piston decreases whereas that along the direction perpendicular to the piston increases, indicating a relaxation of the differential stress. At 873 K, the two apparent pressures merge to the value of the effective hydrostatic pressure, and the differential stress is completely relaxed. Further compression after quenching yields a departure of the two apparent pressures from each other indicating rise of the differential stress as well as the effective hydrostatic pressure in the sample.

Table 1 lists the derived stress (t), parameter α and effective hydrostatic pressure (σ_p) of the sample during the second heating cycle. We notice that the α parameter increases with temperature and becomes >1 at 773 K. This indicates that when large plastic strain accumulates in the sample, Reuss and Voigt limits may not be valid in the polycrystal. A similar phenomenon has been also observed in deformation experiments using neutron diffraction due to different elastic and plastic anisotropy (Daymond et al., 1999). So far, there are very limited experimental data on determining the

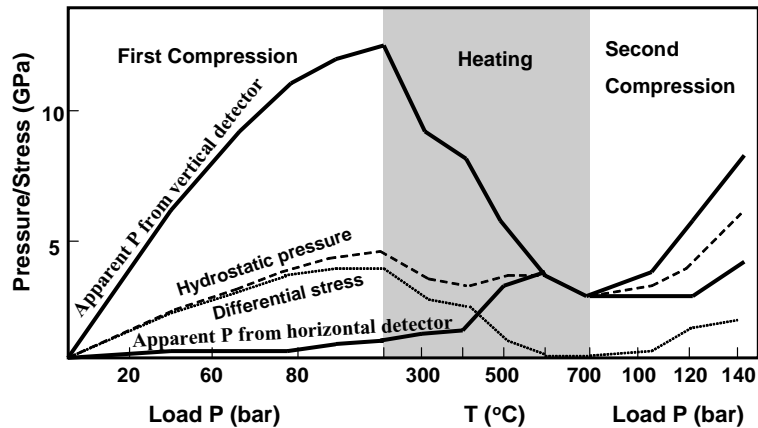


Fig. 9. Apparent pressures calculated from X-ray diffraction at $\psi = 3.2^\circ$ (vertical diffraction) and $\psi = 90^\circ$ (horizontal diffraction), derived hydrostatic pressure and differential stress during first compression, heating at constant load, and continuing compression.

Table 1
Observed stress (t), parameter (α) and effective hydrostatic pressure (σ_p) of fayalite sample during the second heating cycle

T (K)	Pattern #	Time (ks)	t (GPa)	α	σ_p (GPa)
573 (5)	69	25.662	2.7 (1)	0.8 (3)	4.8 (2)
	70	25.877	2.3 (1)	0.7 (3)	4.9 (2)
	71	26.198	2.6 (1)	0.9 (2)	4.9 (2)
	72	28.865	2.2 (1)	0.5 (4)	4.7 (2)
673 (5)	73	29.150	1.9 (1)	0.7 (3)	5.0 (2)
	74	29.426	1.95 (10)	1.0 (2)	4.7 (2)
	75	29.726	2.0 (1)	1.1 (2)	4.5 (2)
	76	30.106	2.0 (1)	1.0 (2)	4.5 (2)
	77	30.340	2.0 (1)	1.0 (2)	4.5 (2)
	78	30.528	1.8 (1)	1.3 (2)	4.6 (2)
773 (5)	79	30.799	1.8 (1)	1.3 (2)	4.4 (2)
	80	30.999	1.7 (1)	1.3 (2)	4.6 (2)
	81	31.199	1.3 (1)	1.3 (2)	4.6 (2)

Note: numbers in parenthesis indicate the experimental uncertainty.

α parameter. Funamori et al. (1994) pioneered such an experiment in a modified Drickamer-type apparatus, and found a decrease of the α parameter from 1 to 0.5 with pressure in NaCl sample. Their experiment was conducted at room temperature. It has not been investigated how the α parameter changes at high temperature when large plastic strain accumulates. In plastic regime, there are also two simplified models, Sachs model (Leffers, 1995; Sachs, 1928) and Taylor model (Bishop and Hill, 1951; Taylor, 1938), describing the coupling between grains in a polycrystal. Similar to Reuss and Voigt models in elastic regime, Sachs and Taylor models assume all the grains in the polycrystal are subjected to the same stress and strain, respectively. However, these models are strongly dependent on the slip systems in each crystal structure, and modeling for olivine phase is not currently available to our knowledge. Data with the α parameter significantly >1 at higher temperature need to be processed with an improved model.

Strain rate versus stress data at 573 and 673 K during the second heating are plotted in Fig. 10. Because deriving strain rate requires two X-ray images taken at a time interval, we use an average of stress over this time period in the plot. Deformation at these low temperatures is dominated by the dislocation glide that is controlled by lattice resistance, and described by Peierls plasticity flow law (Evans and

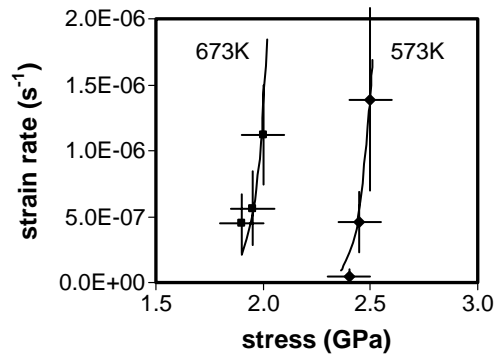


Fig. 10. Strain rate vs. stress of the Fe_2SiO_4 olivine sample at 4.8 GPa, 573 K (solid diamonds) and 4.6 GPa, 673 K (solid squares). Bars attached to the symbols indicate the errors. Solid lines represent the fit lines to the Peierls plasticity flow law (see text) for each data set.

Kohlstedt, 1995)

$$\dot{\epsilon} = \dot{\epsilon}_0 \exp\left(-\frac{Q}{RT} \left(1 - \frac{\sigma}{\tau}\right)^2\right) \quad (16)$$

where $\dot{\epsilon}$ is strain rate, $\dot{\epsilon}_0$ pre-exponential factor (initial strain rate, may be a function of temperature), R the gas constant, T the temperature in Kelvin, Q the activation energy, τ the Peierls stress (lattice friction stress at absolute zero) and σ the stress (the same as t ; for consistency with the literature, we use σ to represent stress in the flow law expression). Fitting the experimental data into this equation, we get $Q = 480 \pm 20$ kJ/mol, $\tau = 6.7 \pm 0.5$ GPa at $\dot{\epsilon}_0 = 1.810^{11} \text{ s}^{-1}$ for $T = 573$ K and $\dot{\epsilon}_0 = 2.3 \times 10^{12} \text{ s}^{-1}$ for $T = 673$ K. The pressure difference between the two temperature data sets is not taken into account during the fitting. Compared with San Carlos olivine data ($Q = 498$ kJ/mol, $\tau = 9.1$ GPa) reported by Evans and Goetze (Evans and Goetze, 1979), our result indicates a weakening by an increase of iron partitioning in olivine structure.

During the third heating cycle, the sample transforms from the olivine to the spinel structure. Interpretation of the X-ray diffraction data from two coexisting phases is in progress. Fig. 11 shows the strain rate versus stress for spinel phase at 873 and 1073 K during the fourth heating cycle. Fitting these data into Eq. (16) yields $Q = 460 \pm 20$ kJ/mol, $\tau = 6.5 \pm 0.5$ GPa at $\dot{\epsilon}_0 = 8.1 \times 10^{13} \text{ s}^{-1}$ for $T = 873$ K and $\dot{\epsilon}_0 = 5.3 \times 10^{15} \text{ s}^{-1}$ for $T = 1073$ K.

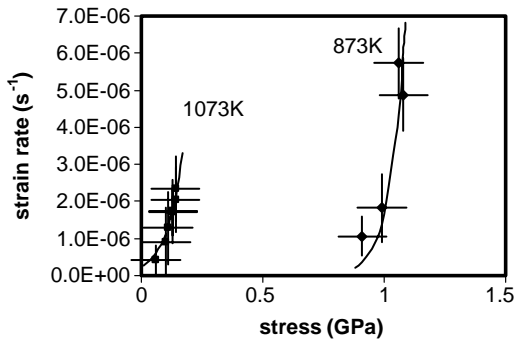


Fig. 11. Strain rate vs. stress of the Fe_2SiO_4 spinel sample at 873 K (solid diamonds) and 1073 K (solid squares) under the pressure of 9 GPa. Bars attached to the symbols indicate the errors. Solid lines represent the fit lines to the Peierls plasticity flow law (see text) for each data set.

Uncertainty in the derived stress relies on the resolution of the X-ray diffraction. In general, the resolution of an energy dispersive diffraction is between 10^{-4} and 10^{-3} , which represents the uncertainty of the experimental lattice elastic strain for stress derivation. Therefore, for the materials with elastic modulus in the order of 10^2 GPa, the uncertainty of stress measurement is about 10–100 MPa. However, another source of uncertainty that can not be quantitatively determined is the inadequacy of the model used to describe the coupling between grains in a real polycrystal. Taking this fact into account, the accuracy of the experimental data might be worse than that discussed here. Uncertainties of the derived parameters by fitting experimental data into an empirical equation are estimated through least square fitting process.

5. Remarks

This study demonstrates that the essential components for constructing a deformation flow law, stress and strain rate, can be attained at high pressure up to 10 GPa and temperature beyond 1000°C by using multi-anvil apparatus in conjunction with synchrotron X-rays. Direct measurements of the strain and stress through sample imaging and X-ray diffraction eliminate the uncertainty introduced in the modeling of indirect measurements at high pressures (e.g. deformation and friction of the pistons that pass the force

to the sample). The X-ray techniques are the critical experimental tools which enable the conventional stress–strain rate deformation experiments at pressures beyond the typical pressure limit of 3 GPa. In addition, the multiple X-ray diffractions as a function of ψ supply very important information for understanding the behavior of high pressure cells in terms of stress distribution in the cell and the response of the cell components to the annealing temperatures. In this study, we find that use of hard pistons to sandwich the sample can generate significant differential stress even after an annealing cycle, and therefore the apparent pressure derived from X-ray diffraction at a given ψ angle (i.e. a common high pressure X-ray diffraction setup) is most likely discrepant from the real pressure. The stress and strain measurement reported here is restricted to a relaxation process. Therefore, the flow law for fayalite derived from the experimental data may not perfectly describe a steady-state flow in the sample. Combined with the developing deformation-DIA type apparatus (Wang et al., 2004), the stress and strain can be measured at a controlled strain rate. One should be able to develop the deformation flow law at a near steady-state.

Acknowledgements

Research carried out (in part) at the National Synchrotron Light Source, Brookhaven National Laboratory, which is supported by the US Department of Energy, Division of Materials Sciences and Division of Chemical Sciences, under Contract No. DE-AC02-98CH10886. We would like to thank Dr. L. Wang and Dr. Z. Zhong for their technical support at the X17 beamline. MPI pub. 314.

References

- Bishop, J.F.W., Hill, R., 1951. A theory of the plastic distortion of a polycrystalline aggregate under combined stresses. *Phil. Mag.* 42, 414.
- Bussod, G.Y., Katsura, T., Rubie, D.C., 1993. The large volume multi-anvil press as a high P – T deformation apparatus. *Pure Appl. Geophys.* 141, 579–599.
- Daymond, M.R., Bourke, M.A.M., Von Dreele, R.B., 1999. Use of Rietveld refinement to fit a hexagonal crystal structure in the presence of elastic and plastic anisotropy. *J. Appl. Phys.* 85 (2), 739–747.

- Durham, W.B., Rubie, D.C., 1998. Can the multianvil apparatus really be used for high-pressure deformation experiments. In: Manghnani, M.H., Yagi, T. (Eds.), *Properties of Earth and Planetary Materials at High Pressure and Temperature*. AGU Geophys. Monogr. 101, 63–70.
- Evans, B., Kohlstedt, D.L., 1995. Rheology of Rocks. *Rock Physics and Phase Relations, A Handbook of Physical Constants*. Washington, DC, AUG, pp. 148–165.
- Evans, B., Goetze, C., 1979. The temperature variation of hardness of olivine and its implication for polycrystalline yield stress. *J. Geophys. Res.* 84, 5505–5524.
- Funamori, N., Yagi, T., Uchida, T., 1994. Deviatoric stress measurement under uniaxial compression by a powder X-ray diffraction method. *J. Appl. Phys.* 75 (9), 4327–4331.
- Graham, E.K., Schwab, J.A., Sopkin, S.M., Takei, H., 1988. The pressure and temperature dependence of the elastic properties of single-crystal fayalite Fe_2SiO_4 . *Phys. Chem. Mineral.* 16, 186–198.
- Green, H.W., Young, T.E., Walker, D., Scholz, C.H., 1990. Anticrack-associated faulting at very high pressure in natural olivine. *Nature* 348, 720–722.
- Hearmon, R.F.S., 1956. The elastic constants of anisotropic materials—II. *Adv. Phys.* 5, 323–382.
- Hofmeister, A.M., Mao, H.K., 2001. Evaluation of shear moduli and other properties of silicates with the spinel structure from IR spectroscopy. *Am. Mineral.* 86, 622–639.
- Karato, S.I., Rubie, D.C., 1997. Toward an experimental study of deep mantle rheology: a new multianvil sample assembly for deformation studies under high pressures and temperatures. *J. Geophys. Res.* 102, 20,111–20,122.
- Kavner, A., Duffy, T.S., 2001. Strength and elasticity of ringwoodite at upper mantle pressures. *Geophys. Res. Lett.* 28 (14), 2691–2694.
- Leffers, T., 1995. Long-range stresses associated with boundaries in deformed materials. *Phys. Stat. Solut.* 149, 69.
- Li, L., Raterron, P., Weidner, D., Chen, J., 2003. Olivine flow mechanisms at 8 GPa. *Phys. Earth Planet. Int.* 138 (2), 113–129.
- Li, L., Weidner, D., Raterron, P., Chen, J., Vaughan, M., 2004. Stress Measurements of Deforming Olivine at High Pressure. *Phys. Earth Planet. Int.* 143–144, 357–367.
- Liebermann, R.C., Wang, Y., 1992. Characterization of sample environment in a multianvil split-sphere apparatus. In: Syono, Y., Manghnani, M.H. (Eds.), *High Pressure Research: Application to Earth and Planetary Sciences*. AGU Geophys. Monogr. 67, pp. 19–31.
- Mao, H.-K., Shu, J., Shen, G., Hemley, R.J., Li, B., Singh, A.K., 1998. Elasticity and rheology of iron above 220 GPa and the nature of the Earth's inner core. *Nature* 396 (6713), 741–743.
- Sachs, G., 1928. Zur Ableitung einer Fließbedingung. *Z. Ver. Deu. Ing.* 72 (22), 734.
- Singh, A.K., 1993. The lattice strain in a specimen (cubic system) compressed nonhydrostatically in an opposed anvil device. *J. Appl. Phys.* 73 (9), 4278–4286.
- Singh, A.K., Balasingh, C., Mao, H.K., Hemley, R.J., Shu, J., 1998. Analysis of lattice strains measured under nonhydrostatic pressure. *J. Appl. Phys.* 83 (12), 7567–7575.
- Taylor, G.I., 1938. Plastic strain in metals. *J. Inst. Metals* 62, 307.
- Tingle, T.N., Green II, H.W., Young, T.E., Koczyński, T.A., 1993. Improvements to Griggs-type apparatus for mechanical testing at high pressures and temperatures. *Pure Appl. Geophys.* 141, 523–543.
- Uchida, T., Funamori, N., Yagi, T., 1996. Lattice strains in crystals under uniaxial stress field. *J. Appl. Phys.* 80 (2), 739–746.
- Uchida, T., Yagi, T., Funamori, N., Anonymous, 1997. Differential stress in Mg_2SiO_4 under uniaxial stress field; variation with pressure, temperature, and phase transformation. *American Geophysical Union, 1997 fall meeting* 78 (Suppl. 46) 722.
- Vaughan, M.T., Weidner, D.J., Wang, Y.B., Chen, J.H., Koleda, C.C., Getting, I.C., 1998. T-cup: A new high-pressure apparatus for X-ray studies. *Rev. High Pressure Sci. Technol.* 7, 1520–1522.
- Wang, Y., Durham, W.B., Getting, I.C., 2004. D-DIA: A new apparatus for triaxial deformation at pressures up to 15 GPa, this volume.
- Weidner, D.J., 1998. Rheological studies at high pressure. In: Hemley, R.J. (Ed.), *Ultra-high-Pressure Mineralogy: Physics and Chemistry of the Earth's Deep Interior*, vol. 37. Mineralogical Society of America, Washington, DC, pp. 493–524.
- Weidner, D.J., Wang, Y., Chen, G., Ando, J., Vaughan, M.T., 1998. Rheology measurements at high pressure and temperature. In: Manghnani, M.H., Yagi, T. (Eds.), *Properties of earth and planetary materials at high pressure and temperature*. AGU Geophys. Monogr. 101, 473–482.
- Yamazaki, D., Kato, T., Ohtani, E., 1996. Preferred orientation of olivine in stress field under ultra-high pressures. *J. Seismol. Soc. Jpn.* 49, 39–53.
- Yamazaki, D., Karato, S., 2001. High-pressure rotational deformation apparatus to 15 GPa. *Rev. Sci. Instrum.* 72 (11), 4207–4211.